Reactive force field development for magnesium chloride hydrates and its application for seasonal heat storage†

Amar Deep Pathak,*[a] Silvia Nedea,[a] Adri C. T. van Duin,[b] Herbert Zondag,[a] Camilo Rindt[a] and David Smeulders[a]

$MgCl_2$ hydrates are considered as high-potential candidates for seasonal heat storage materials. These materials have high storage capacity and fast dehydration kinetics. However, as a side reaction to dehydration, hydrolysis may occur. Hydrolysis is an irreversible reaction, which produces HCl gas thus affecting the durability of heat storage systems. In this study, we present the parameterization of a reactive force field (ReaxFF) for $MgCl_2$ hydrates to study the dehydration and hydrolysis kinetics of $MgCl_2 \cdot H_2O$ and $MgCl_2 \cdot 2H_2O$. The ReaxFF parameters have been derived by training against quantum mechanics data obtained from Density Functional Theory (DFT) calculations consisting of bond dissociation curves, angle bending curves, reaction enthalpies, and equation of state. A single-parameter search algorithm in combination with a Metropolis Monte Carlo algorithm is successfully used for this ReaxFF parameterization. The newly developed force field is validated by examining the elastic properties of $MgCl_2$ hydrates and the proton transfer reaction barrier, which is important for the hydrolysis reaction. The bulk moduli of $MgCl_2 \cdot H_2O$ and $MgCl_2 \cdot 2H_2O$ obtained from ReaxFF are in close agreement with the bulk moduli obtained from DFT. A barrier of 20.24 kcal mol^{-1} for the proton transfer in $MgCl_2 \cdot 2H_2O$ is obtained, which is in good agreement with the barrier (19.55 kcal mol^{-1}) obtained from DFT. Molecular dynamics simulations using the newly developed ReaxFF on 2D-periodic slabs of $MgCl_2 \cdot H_2O$ and $MgCl_2 \cdot 2H_2O$ show that the dehydration rate increases more rapidly with temperature in $MgCl_2 \cdot H_2O$ than in $MgCl_2 \cdot 2H_2O$, in the temperature range 300–500 K. The onset temperature of HCl formation, a crucial design parameter in seasonal heat storage systems, is observed at 340 K for $MgCl_2 \cdot H_2O$, which is in agreement with experiments. The HCl formation is not observed for $MgCl_2 \cdot 2H_2O$. The diffusion coefficient of H_2O through $MgCl_2 \cdot H_2O$ is lower than through $MgCl_2 \cdot 2H_2O$, and can become a rate-limiting step. The diffusion coefficient increases with temperature and follows the Arrhenius law both for $MgCl_2 \cdot H_2O$ and $MgCl_2 \cdot 2H_2O$. These results indicate the validity of the ReaxFF approach for studying $MgCl_2$ hydrates and provide important atomistic-scale insight of reaction kinetics and H_2O transport in these materials.

1 Introduction

Thermal energy storage is necessary for the successful implementation of solar thermal energy.[1] Solar thermal energy can be stored in three forms: sensible, latent, and thermochemical.[2] Thermal storage is a proven concept but it is volume restricted. The energy storage density is higher in thermochemical form than in sensible or latent form. Therefore thermochemical materials (TCMs) may offer a compact seasonal heat storage solution.[3]

Salt hydrates are one class of TCMs.[1] These materials convert thermal energy (physical form of energy) into chemical form by decomposing into lower hydrate form or anhydrous form (charging cycle). Anhydrous and lower hydrates recombine with water vapor (present in moisture) to form hydrates again, thereby releasing energy (discharging cycle). The operating principle of TCM can be expressed with the following reaction:

$$\text{Salt} \cdot m\text{H}_2\text{O} + \text{Heat} \leftrightarrow \text{Salt} \cdot (m-n)\text{H}_2\text{O} + n\text{H}_2\text{O}.$$

In addition to higher energy storage capacity, TCMs can store thermal energy with almost no heat loss, even for longer periods, making TCM a unique seasonal heat storage material.[4,5] Selection of an appropriate salt hydrate is the key aspect in designing a thermochemical heat storage system.[6] Halide based salt hydrates ($CaX_2 \cdot 6H_2O$, $MgX_2 \cdot 6H_2O$, and $SrX_2 \cdot 6H_2O$,

[a] *Energy Technology, P.O. Box 513, 5600 MB Eindhoven, The Netherlands.*
  E-mail: a.d.pathak@tue.nl
[b] *Department of Mechanical and Nuclear Engineering, Pennsylvania State University, 240 Research East Building, University Park, PA 16802, USA*
† Electronic supplementary information (ESI) available. See DOI: 10.1039/c6cp02762h

15838 | *Phys. Chem. Chem. Phys.*, 2016, **18**, 15838–15847

This journal is © the Owner Societies 2016

X = Cl/Br), sulphate based salt hydrates (LiSO$_4$·H$_2$O, MgSO$_4$·7H$_2$O), and nitrate based salt hydrates (LiNO$_3$·3H$_2$O, Zn(NO$_3$)$_2$·3H$_2$O) are the major class of promising reversible TCMs.[6] These hydrates have theoretical crystal storage capacities between 2–3 GJ m^{-3}.[6]

Magnesium chloride hydrates (MgCl$_2$·nH$_2$O, n = 0, 1, 2, 4, and 6) have been investigated extensively as an appropriate candidates for solar thermal storage.[7–13] MgCl$_2$·6H$_2$O (Bischofite) has been successfully tested for 1000 cycles for application in solar based cooking.[11] Thermal dehydration of Bischofite is an important process in production of pure Mg, Mg alloys, MgO, and in heat storage applications.[14–17] The dehydration kinetics for MgCl$_2$ hydrates is faster than for other materials like MgSO$_4$ hydrates,[8,18] but a problem with this material is the presence of the hydrolysis along with the dehydration. Hydrolysis is an irreversible side reaction in the dehydration process, which produces HCl gas and affects the durability of the heat storage system. It was experimentally observed that the hydrolysis reaction could be avoided by use of external HCl pressure[14] or by adding other halides.[19] However, there is no fundamental understanding of the conditions for the hydrolysis.

Next to the dehydration, the HCl production is also a key aspect in designing the MgCl$_2$ based heat storage system. Experimentally, thermal dehydration and hydrolysis of MgCl$_2$ hydrates have been studied by thermogravimetric analysis (TGA),[17] derivative thermogravimetry (DTG),[20] TGA/Differential scanning calorimetry (DSC)[10] and thermochemical analysis.[14] Galwey et al.[21] has experimentally observed the hydrolysis reaction in MgCl$_2$·2H$_2$O in the temperature range of 623–703 K.[21] Kirsh et al.[20] has not observed hydrolysis below 473 K for MgCl$_2$ hydrates, but found 43.8% of chlorine released as HCl at 673 K. However, Huang et al.[17] has reported the onset temperature of HCl formation at 440 K in MgCl$_2$·2H$_2$O. Kipouros et al.[14] has reported hydrolysis at 417 K for MgCl$_2$·2H$_2$O and at 413 K for MgCl$_2$·H$_2$O for an equilibrium HCl pressure of 5 × 10^{-3} atm. The onset temperature of HCl formation is thus ambiguous from experiments. There is no theoretical study to determine the hydrolysis kinetics and the onset temperature of HCl formation.

Atomic and molecular level simulations turned to be useful tools to gain insight in the hydrolysis coupled dehydration reactions. Weck et al.[12] has computed thermal properties from thermodynamical calculations of MgCl$_2$·nH$_2$O using Density Function Theory (DFT) under harmonic assumption. Wang et al.[16] has considered MgCl$_2$·H$_2$O to be the potential candidate for hydrolysis and proposed a reaction path for thermolysis of MgCl$_2$·H$_2$O from DFT calculations. Smeets et al.[8] has obtained the safety limit of hydrolysis reactions for all hydrates of MgCl$_2$ from DFT calculations using equilibrium thermodynamic principles under the ideal poly-atomic gas assumption. The atomic scale calculations can simulate systems upto a system size of 100–1000 atoms and a time scale upto 200 picosecond over a week of high performance computing.[22] To the best of our knowledge, no kinetic study was done on molecular level to investigate the hydrolysis and dehydration reactions of MgCl$_2$·H$_2$O and MgCl$_2$·2H$_2$O from first principle atomic level calculations, integrating the quantum level results to molecular level modeling under reactive force field (ReaxFF) formalism.

For an efficient TCM storage cycle, heat and mass transfer in the storage volume are essential.[2] Experimentally it has been observed that water transport through the solid MgCl$_2$ hydrate affects the dehydration rate and may become the rate limiting step under specific reaction conditions.[23] To understand the complex reaction (hydration and dehydration) coupled with water transport, it is desirable to investigate the diffusive transport of water molecules, which are formed by the dehydration reaction. These water molecules have to diffuse to the surface of the solid salt hydrate. The diffusion path may vary from several atomic layers up to a few micrometer.[24] The water transport through the solid salt hydrate, the temperature, the diffusion path length, the external H$_2$O pressure and the crystal defects influence considerably the dehydration rate.[25] To study the effect of these aspects on the complex dehydration reaction on molecular level, a force field is required that is able to capture both the chemical reactivity and the mass transport of H$_2$O in MgCl$_2$·H$_2$O and MgCl$_2$·2H$_2$O crystals.

Chemical reactivity has been incorporated using bond order dependent ReaxFF.[26,27] According to previous studies,[28,29] a training set needs to be developed from quantum level DFT calculations consisting of the bond dissociation energy curves of Mg–Cl and Mg–O bonds, the angle bending energy curves of Cl–Mg–Cl, O–Mg–O, and O–Mg–Cl angles in gaseous hydrates, the reaction enthalpies of dehydration and hydrolysis reaction, and the condensed phase equation of state (EOS) of MgCl$_2$, MgCl$_2$·H$_2$O and MgCl$_2$·2H$_2$O.[27,30,31] To our knowledge, no DFT studies exist presenting this information of the MgCl$_2$ hydrates. For this purpose, in this paper we obtained various molecular structures of MgCl$_2$ hydrates, reaction enthalpies, bond dissociation energies, angle bending energies, and EOS from DFT. With this extended information, we parameterize a new force field for MgCl$_2$ hydrates. Both a single-parameter search algorithm[32] and a Metropolis Monte Carlo (MMC) algorithm[33] are used to optimize the newly developed ReaxFF for investigated MgCl$_2$ hydrates.

In the present study, we parameterize the ReaxFF to model the dehydration kinetics of MgCl$_2$·H$_2$O and MgCl$_2$·2H$_2$O, as these hydrates are prone to hydrolysis reactions. Proton transfer is an important step in the hydrolysis reaction. The energy barrier for proton transfer in MgCl$_2$·2H$_2$O is obtained from the ReaxFF simulations and validated against results from DFT. The extent of the reaction depends on the temperature of the solid and the vapor transport inside the solid. The new ReaxFF is used to study the effect of temperature on the dehydration in the temperature range of 300–500 K. This temperature range is the typical operating range of TCM based heat storage systems. The onset temperature of HCl formation is investigated in the same temperature range. The dependence of the diffusion coefficient (DC) on temperature is analyzed using the Green–Kubo (GK) method.

2 Computational methods

2.1 Quantum mechanics calculations

To accurately predict the dehydration and hydrolysis reaction in the condensed phase of MgCl$_2$ hydrates, quantum mechanics (QM) calculations are performed in both periodic and non-periodic

This journal is © the Owner Societies 2016

Phys. Chem. Chem. Phys., 2016, **18**, 15838–15847 | **15839**

systems in order to generate a training set necessary to parameterize the new force field. DFT under the generalized gradient approximation (GGA) is used for the QM calculations. All the non-periodic $MgCl_2$ hydrate clusters are relaxed in the framework of DFT implemented in Amsterdam Density Functional (ADF) program.[34] The Perdew–Wang exchange and correlation functional (PW91) is used with a double polarized triple-ζ basis set. A similar GGA-DFT framework has been used to study the $CaCl_2$, $MgCl_2$, and $MgSO_4$ hydrates.[8,18,35] The bond dissociation energy for Mg–O and Mg–Cl bonds are obtained from GGA-DFT for $MgCl_2 \cdot H_2O$ and $MgCl_2 \cdot 2H_2O$ as they are responsible for the hydrolysis and the dehydration reactions. Similarly, the angle bending energy curves in $MgCl_2$ hydrates like O–Mg–O, Cl–Mg–Cl, H–O–Mg are also obtained from GGA-DFT.

To simulate a reaction in solid phase of hydrates, the crystal structure of $MgCl_2$, $MgCl_2 \cdot H_2O$, and $MgCl_2 \cdot 2H_2O$ are compressed or stretched uniformly upto 20–30% of their relaxed volume to obtain the EOS. The periodic systems are relaxed in the framework of GGA-DFT using the VASP package.[36] The projector augmented wave (PAW) method[37] along with the Perdew Burke Ernzerhof (PBE) exchange–correlation functional[38] is used under the GGA approximation. The Monkhorst–Pack k-point mesh is used to integrate the Brillouin zone of $MgCl_2$ ($5 \times 5 \times 3$), $MgCl_2 \cdot H_2O$ ($3 \times 5 \times 3$), and $MgCl_2 \cdot 2H_2O$ ($4 \times 4 \times 8$). The unit cell of crystals are fully relaxed with break condition for ionic relaxation of 10^{-6} eV and plane wave cut off of 500 eV using tetrahedron method with Blöchl corrections.

2.2 Reactive force field and parameterization

ReaxFF is a general bond-order-dependent many body empirical potential with a polarizable charge model that dynamically predicts a bond formation and dissociation during a reaction without connecting step function potentials.[39] ReaxFF formalism represents a continuous landscape of energy which is dependent on the bond order and the non-bonded distance. The bond order is obtained from the inter-atomic distance and energy contribution updated with time. In the ReaxFF formalism, the total energy of the system can be partitioned into the following terms:

$$E_{total} = E_{bond} + E_{val} + E_{tor} + E_{lp} + E_{over/under} + E_{conj}$$
$$+ E_{H-bond} + E_{others} + E_{Coulomb} + E_{vDW}. \quad (1)$$

E_{total} is the overall interaction energy of the system, $E_{Coulomb}$ is the electrostatic contribution, and E_{bond} is the bond energy. E_{val} and E_{tor} are the three-body valence angle terms and the four-body torsion terms respectively. E_{lp} and $E_{over/under}$ are the energy contributions from lone-pair electrons, and the penalty energy coming from over coordination and under coordination, E_{conj} represents the conjugation energy term, E_{H-bond} represents the weak hydrogen bond and E_{others} is introduced for other correcting types of species. $E_{Coulomb}$ and E_{vDW} are the non-bonded interactions between all pairs irrespective of the connectivity in the system. The Coulomb charge is calculated dynamically from the electro-negativity equalization method.[39] Excessive electrostatic repulsions at very short interatomic distance are avoided by shielding parameters.

The ReaxFF parameters required to define the potential energy surface are optimized against the training set obtained from QM data. The initial O/H parameters are taken from the iron–oxyhydroxide force field.[40] The O/H parameters are kept fixed while bond parameters of Mg–O, Mg–Cl and angle parameters associated with these Mg and Cl are optimized. The optimization is done in such a way that optimized parameters are able to reproduce the energy and structural data present in the training set. The data in the training set used for comparison include bond dissociation energy, angle bending curve, reaction enthalpy and EOS for $MgCl_2$, $MgCl_2 \cdot H_2O$, and $MgCl_2 \cdot 2H_2O$. In an optimization process, ReaxFF parameters are varied such that the cumulative error (Ξ) between the DFT data in the training set and their corresponding values obtained from ReaxFF is minimized. The cumulative error is defined as

$$\Xi = \sum_{i=1}^{n} \left[\frac{X_{i,DFT} - X_{i,ReaxFF}}{\sigma_i} \right]^2. \quad (2)$$

In this equation, $X_{i,DFT}$ is the DFT value in the training set for data point i, and $X_{i,ReaxFF}$ is the corresponding value obtained by ReaxFF. σ_i is a weight assigned to the ith data point to set its relative importance compared to other data points. In a single-parameter search algorithm,[32] a parabolic extrapolation method is used for parameterization. Further, we have used an MMC algorithm[33] to attain global minima of the cumulative error as ReaxFF parameters are correlated. In the MMC algorithm multiple parameters are changed with a random movement at every iteration and the proposed configuration is accepted with a probability given by

$$P = \min \left[1, \exp^{-\left(\frac{E_{old} - E_{new}}{k_B T} \right)} \right]. \quad (3)$$

E_{new} is the error from the new set of parameter proposition and E_{old} from the old set. T is an artificial temperature which gradually decreases after each iteration (simulated annealing) and k_B is the Boltzmann constant. The MMC algorithm has shown a good agreement between QM and ReaxFF data for $MgSO_4$ hydrates systems.[33]

2.3 Diffusion

The DC of H_2O molecules through the $MgCl_2$ hydrate crystal is obtained from the GK formulation described as

$$D = \frac{1}{3} \int_0^\infty \langle v(t) \cdot v(0) \rangle dt. \quad (4)$$

D is the diffusion coefficient of water molecules. The expression $\langle v(t) \cdot v(0) \rangle$ is known as the velocity autocorrelation function (VAF).[41] The DC of H_2O molecules through the $MgCl_2$ hydrate crystals is obtained in a spherical control volume of radius R in such a way that the crystal slab resides completely in the sphere and the center of mass of this slab is chosen as the center of the sphere as shown in Fig. 9. The motion of the relatively heavy O atom in a water molecule determines the trajectory of the H_2O molecule as the center of mass of the H_2O molecule coincides with that of the O atom.

15840 | *Phys. Chem. Chem. Phys.*, 2016, **18**, 15838–15847

This journal is © the Owner Societies 2016

3 Results and discussion

3.1 Force field parameterization results

The initial force field parameters are optimized against hydrated Cl^- ion and $MgCl_2$ condensed phase data. The bond dissociation energies for Mg–Cl and Mg–O bonds present in $MgCl_2$, $MgCl_2 \cdot H_2O$, and $MgCl_2 \cdot 2H_2O$ gas molecules are obtained from restrained GGA-DFT calculations. Bond dissociation energy is the relative energy of the constrained molecule (specific bond constrain) with respect to its relaxed geometry. Similarly, angle bending curves for Cl–Mg–Cl, O–Mg–O, O–Mg–Cl, and H–O–Mg are obtained from GGA-DFT. The single-parameter search algorithm[32] approaches a global minimum when the initial ReaxFF parameters are chosen close to that minimum while the multi-parameter MMC algorithm[33] approaches the global minimum irrespective of the initial guess. The bond and angle parameters are optimized with the single-parameter search[32] followed by the multi-parameter MMC algorithm[33] such that the trained parameters can reproduce the training set data accurately and the cumulative error attains a global minimum.

The optimized ReaxFF parameters are able to reproduce the bond dissociation curve of Mg–O and Mg–Cl bond present in $MgCl_2 \cdot H_2O$ and $MgCl_2 \cdot 2H_2O$ as shown in Fig. 1 and 2 remarkably well, particularly near the minimum. The shape of the Mg–O dissociation curve obtained from ReaxFF slightly differs from the DFT one. This discrepancy can be explained from the fact that there are many conformers of similar energy existing at the same Mg–O distance due to the weak bonded interaction of H_2O with $MgCl_2$ and to the relatively strong non-bonded interaction in $MgCl_2 \cdot H_2O$ and $MgCl_2 \cdot 2H_2O$. The optimized ReaxFF is also able to capture the angle bending energy curves for $MgCl_2 \cdot H_2O$ and $MgCl_2 \cdot 2H_2O$ (see ESI†). The enthalpy change in the dehydration and in the hydrolysis reactions (gas phase) for $MgCl_2 \cdot H_2O$ and $MgCl_2 \cdot 2H_2O$ are obtained from DFT. ReaxFF is also able to capture the enthalpy change in the dehydration and hydrolysis reaction of $MgCl_2 \cdot H_2O$ and $MgCl_2 \cdot 2H_2O$ with a maximum difference of 5.5 kcal mol^{-1} (28% of DFT value) as shown in Fig. 3.

To predict the kinetics of solid $MgCl_2 \cdot H_2O$ and $MgCl_2 \cdot 2H_2O$, the EOS is essential. The optimized force field, which is able to describe the gas phase reactions accurately, is further optimized with
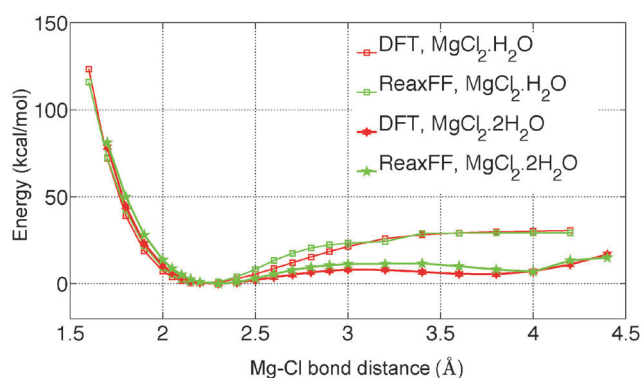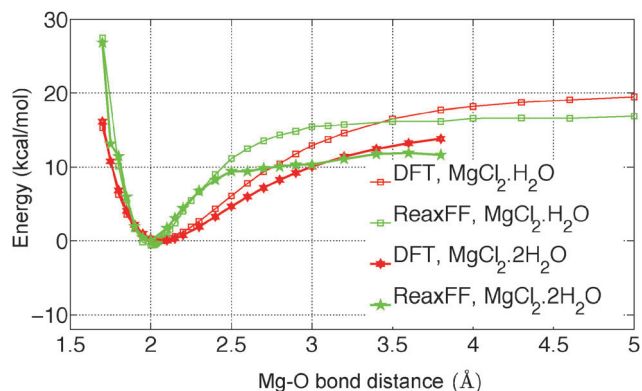

Fig. 2 Comparison of the Mg−O bond dissociation energy curve in $MgCl_2$ hydrates obtained from DFT and ReaxFF.

a condensed phase EOS of $MgCl_2$ hydrates obtained from DFT in VASP.[36] The parameterized force field is also able to predict the experimentally observed crystal structures of $MgCl_2$,[42] $MgCl_2 \cdot H_2O$,[43] and $MgCl_2 \cdot 2H_2O$[44] as shown in Table 1. In Table 1 (rows 1–6), it can be observed that ReaxFF reproduces the lattice parameters of the unit cell of $MgCl_2$, $MgCl_2 \cdot H_2O$ and $MgCl_2 \cdot 2H_2O$ with great accuracy. ReaxFF is also able to reproduce the EOS for $MgCl_2$, $MgCl_2 \cdot H_2O$ and $MgCl_2 \cdot 2H_2O$ as shown in Fig. 4–6.

The bulk modulus is obtained from fitting the Birch–Murnaghan equation of state with the EOS obtained from DFT and ReaxFF. The bulk modulus (B_0) and its first order derivative with respect to pressure ($B_0{}'$) (rows 7 and 8 of Table 1) is obtained from ReaxFF and found to be in good agreement with DFT results for $MgCl_2$, $MgCl_2 \cdot H_2O$ and $MgCl_2 \cdot 2H_2O$.

3.2 Proton transfer reaction

Hydrolysis is an irreversible reaction which is usually observed in $MgCl_2 \cdot H_2O$ and $MgCl_2 \cdot 2H_2O$. Wang and Chen[16] have studied the thermolysis mechanism of $MgCl_2 \cdot H_2O$ using a semi-empirical PM3 method. They observed that proton transfer is an important step in the hydrolysis reaction. To understand the reaction path for the proton transfer in $MgCl_2 \cdot 2H_2O$, the relative energy of a

Fig. 1 Comparison of the Mg−Cl bond dissociation energy curve in $MgCl_2$ hydrates obtained from DFT and ReaxFF.
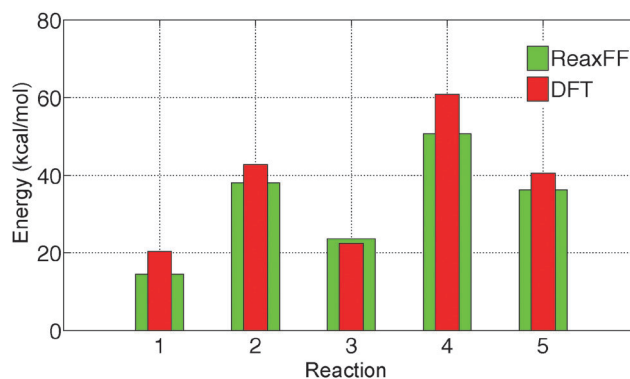

Fig. 3 Comparison of change in reaction enthalpy for the dehydration and the hydrolysis reactions obtained from DFT and ReaxFF. The indices on the X axis represent the following reactions: (1) $MgCl_2 \cdot 2H_2O \rightarrow MgCl_2 \cdot H_2O + H_2O$ (2) $MgCl_2 \cdot 2H_2O \rightarrow MgCl_2 + 2H_2O$ (3) $MgCl_2 \cdot H_2O \rightarrow MgCl_2 + H_2O$ (4) $MgCl_2 \cdot 2H_2O \rightarrow MgOHCl + HCl + H_2O$ (5) $MgCl_2 \cdot H_2O \rightarrow MgOHCl + HCl$.

This journal is © the Owner Societies 2016

Phys. Chem. Chem. Phys., 2016, **18**, 15838–15847 | **15841**

Table 1 Comparison of computed lattice parameters and elastic properties of $MgCl_2$, $MgCl_2 \cdot H_2O$, and $MgCl_2 \cdot 2H_2O$ from DFT and ReaxFF. The value given in the parenthesis represents the experimental data[42–44]

	$MgCl_2$		$MgCl_2 \cdot H_2O$		$MgCl_2 \cdot 2H_2O$	
	ReaxFF	DFT	ReaxFF	DFT	ReaxFF	DFT
a (Å)	3.665	3.662 [3.596][42]	8.936	8.936 [8.917][43]	7.649	7.672 [7.389][44]
b (Å)	3.665	3.666 [3.596][42]	3.691	3.692 [3.634][43]	8.491	8.516 [8.550][44]
c (Å)	19.860	19.840 [17.589][42]	11.592	11.593 [11.477][43]	3.694	3.705 [3.648][44]
α (°)	90	90 [90][42]	90	90 [90][43]	90	90 [90]
β (°)	90	90 [90][42]	90	90 [90][43]	102.46	102.45 [98.96]
γ (°)	120	120 [90][42]	90	90 [90][43]	90	90 [90]
B_0 (GPa)	19.28	17.54	20.51	21.02	24.65	23.66
$B_0{}'$	3.65	4.03	6.84	6.31	6.38	5.96
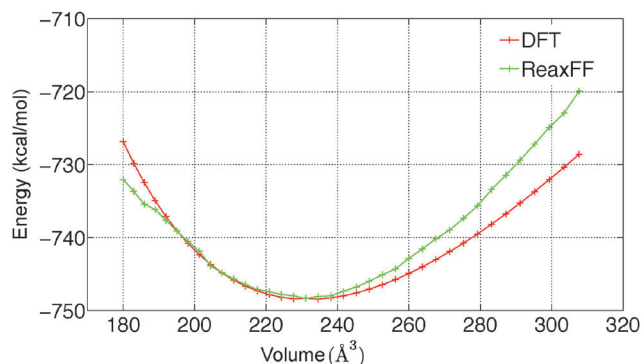
Fig. 4 Comparison of the EOS for $MgCl_2$ obtained from DFT and ReaxFF.

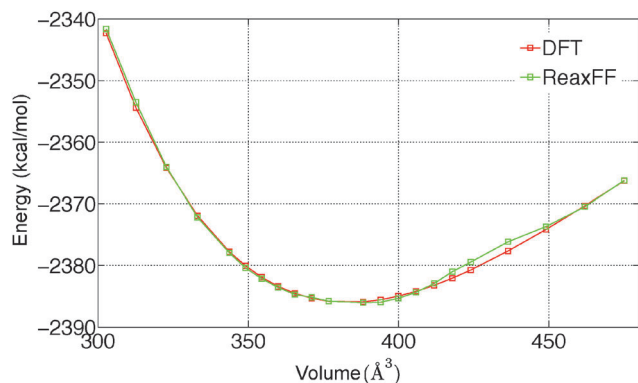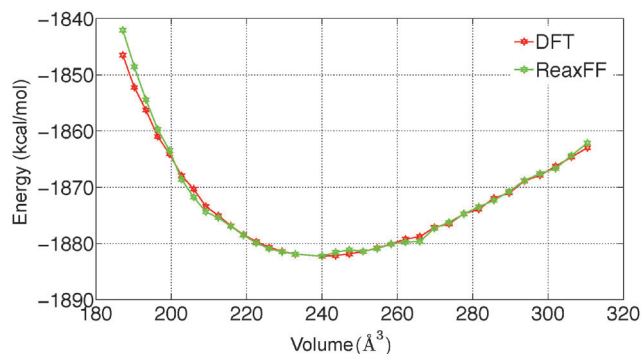**Fig. 5** Comparison of the EOS for $MgCl_2 \cdot H_2O$ obtained from DFT and ReaxFF.

Fig. 6 Comparison of the EOS for $MgCl_2 \cdot 2H_2O$ obtained from DFT and ReaxFF.

$MgCl_2 \cdot 2H_2O$ molecule is obtained from GGA-DFT calculations by constraining the O–H bond lengths, which is shown in Fig. 7(a). We obtained a barrier of 19.55 kcal mol^{-1} for proton transfer in gaseous $MgCl_2 \cdot 2H_2O$ and a barrier of 8.31 kcal mol^{-1} for chloride ion (Cl$^-$) formation, which indicates that proton transfer is a rate determining step in the hydrolysis reaction. To validate the applicability of the ReaxFF, we obtained the reaction path for proton transfer in gaseous $MgCl_2 \cdot 2H_2O$ from ReaxFF and compared it with DFT. From Fig. 8, it can be observed that ReaxFF is able to predict the barrier for proton transfer (20.24 kcal mol^{-1}) and the reaction coordinate for proton transfer in $MgCl_2 \cdot 2H_2O$.

To understand the effect of a neighboring H_2O molecule in proton transfer of $MgCl_2 \cdot 2H_2O$, a H_2O molecule is placed nearby as shown in Fig. 7(b). A barrier of 29.61 kcal mol^{-1} is obtained from DFT for proton transfer in $MgCl_2 \cdot 2H_2O$ surrounded by one H_2O molecule. This explains the lower hydrolysis in the higher hydrates (tetra and hexa) of $MgCl_2$, as the neighboring H_2O molecule increases the barrier for proton transfer and inhibits the hydrolysis. A barrier of 26.54 kcal mol^{-1} for proton transfer is obtained from ReaxFF, which is in agreement with the DFT result (29.61 kcal mol^{-1}). The position of the transition state predicted from ReaxFF differs by 0.5 Å because surrounding H_2O molecule may form many structures of similar energy (see ESI†).

3.3 ReaxFF-MD simulations of $MgCl_2$ hydrates

In the present study, we have investigated the kinetics of dehydration and hydrolysis reactions of solid $MgCl_2 \cdot H_2O$ and $MgCl_2 \cdot 2H_2O$.

(a) $MgCl_2 \cdot 2H_2O$ **(b)** $MgCl_2 \cdot 2H_2O + H_2O$

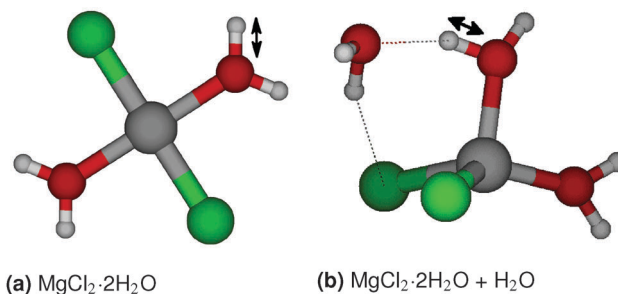**Fig. 7** The initial optimized structure of $MgCl_2 \cdot 2H_2O$ molecules used to obtain the reaction path of proton transfer from DFT and ReaxFF. $MgCl_2 \cdot 2H_2O$ is represented using the ball-and-stick model. Color scheme: Mg = grey, O = red, H = white, and Cl = green.
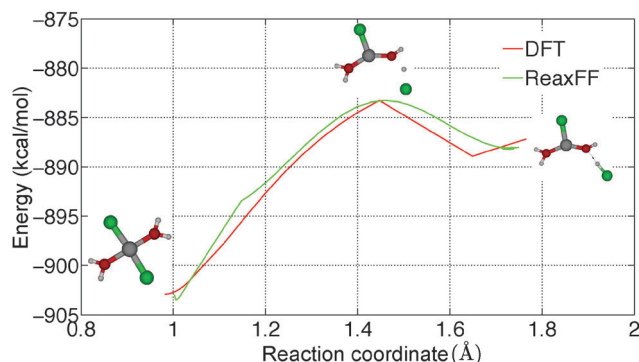
Fig. 8 Comparison of barriers for proton transfer in $MgCl_2 \cdot 2H_2O$ obtained from DFT and ReaxFF. $MgCl_2 \cdot 2H_2O$ is represented using the ball-and-stick model. Color scheme: Mg = grey, O = red, H = white, and Cl = green.

We created the $3 \times 6 \times 6$ super-cell of $MgCl_2 \cdot H_2O$ crystal[43] and $6 \times 6 \times 6$ super-cell of $MgCl_2 \cdot 2H_2O$[44] from their experimental crystallographic information file (CIF).[45] 2D-periodic slabs of $26.8 \times 21.8 \times 1000$ Å for $MgCl_2 \cdot H_2O$ (as shown in Fig. 13a) and $44.3 \times 1000 \times 21.9$ Å for $MgCl_2 \cdot 2H_2O$ (as shown in Fig. 9a) are prepared from the super-cell by eliminating periodicity in the Z and Y direction respectively. The removal of periodicity is chosen is a direction parallel to the Mg–O bond as the Mg–O bond is weaker than the Mg–Cl bond. We carried out *NVT*-MD simulations at various temperatures using the Berendsen thermostat with a temperature damping constant of 100 femtosecond. The MD time step of 0.25 femtosecond is used for $MgCl_2 \cdot H_2O$ and $MgCl_2 \cdot 2H_2O$. All simulations are performed upto 1 nanosecond and average number of molecules are recorded from last 500 picosecond.

3.3.1 Force field validation. To validate ReaxFF, the radial distribution function (RDF) calculated from the MD simulations (upto 250 picosecond) for O–H, Mg–O, and Mg–Cl in 2D periodic slabs of $MgCl_2 \cdot H_2O$, $MgCl_2 \cdot 2H_2O$ are calculated and shown in Fig. 10. The peak location for O–H pair is observed at 1.02 Å

which is close to the O–H bond length (0.98 Å) reported earlier in the experimental unit cell of $MgCl_2 \cdot H_2O$.[43] A similar peak location was reported from the ReaxFF parameters of Lindqvist Polyoxoanion in Bulk Water.[46]

The first peak location for the Mg–O pair is observed at 2.0 Å, which represents the Mg–O atomic bond as shown in Fig. 10. The corresponding distance in the experimental unit cell of $MgCl_2 \cdot 2H_2O$ is 2.0 Å.[44] The second peak location for Mg–O pair is observed at 4.4 Å, which represents the non-bonded Mg attractions with the H_2O molecule of the adjacent $MgCl_2$ hydrate as shown in Fig. 10. The corresponding distance in the experimental unit cell of $MgCl_2 \cdot 2H_2O$ is 4.0 Å[44] in this case.

The first peak location for Mg–Cl pair is observed at 2.3 Å which represents the Mg–Cl bond. The corresponding distances in the experimental unit cell of $MgCl_2 \cdot H_2O$ and $MgCl_2 \cdot 2H_2O$ are 2.56 Å.[43,44] The second peak is observed at 4.3 Å and 4.7 Å for $MgCl_2 \cdot H_2O$ and $MgCl_2 \cdot 2H_2O$ which represents the Mg attraction with Cl of the adjacent $MgCl_2$ hydrate molecule as shown in Fig. 10. The corresponding distances in the experimental unit cell of $MgCl_2 \cdot H_2O$ and $MgCl_2 \cdot 2H_2O$ are 4.5 Å[43] and 4.8 Å,[44] respectively. We conclude that ReaxFF parameters obtained from the present study are consistent with DFT results and experimental results in representing the bonded and non-bonded interactions.

3.3.2 Dehydration reaction. The dehydration kinetics of $MgCl_2 \cdot H_2O$ and $MgCl_2 \cdot 2H_2O$ are investigated at various temperature (300, 350, 400, 450, and 500 K). This temperature range falls in the operating range of the TMC based seasonal heat storage systems. The average number of H_2O molecules leaving from the solid slab of $MgCl_2 \cdot H_2O$ ($26.8 \times 21.8 \times 1000$ Å) into the vacuum region (Z direction) is 21.38 ± 4.45 after 1000 picosecond at 300 K. The average number of H_2O molecules escaping from $MgCl_2 \cdot H_2O$ increases from 21.28 ± 4.45 to 75.43 ± 9.08 in the temperature range of 300 to 500 K as shown in Fig. 11. A molecular dehydration rate could be estimated from
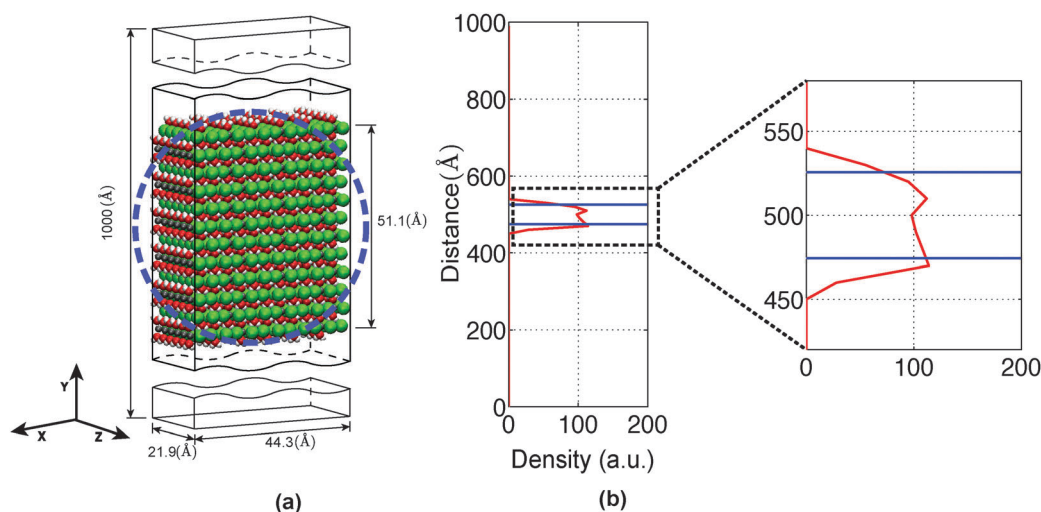

Fig. 9 A 2D periodic slab of $MgCl_2 \cdot 2H_2O$ is used for ReaxFF-MD simulations (a) the initial configuration, the blue dotted sphere represents a control volume used for H_2O diffusion using GK method. $MgCl_2 \cdot 2H_2O$ is represented using the ball-and-stick model. Color scheme: Mg = grey, O = red, H = white, and Cl = green (b) average density distribution of H_2O along the Y axis after 375 ps at 300 K.
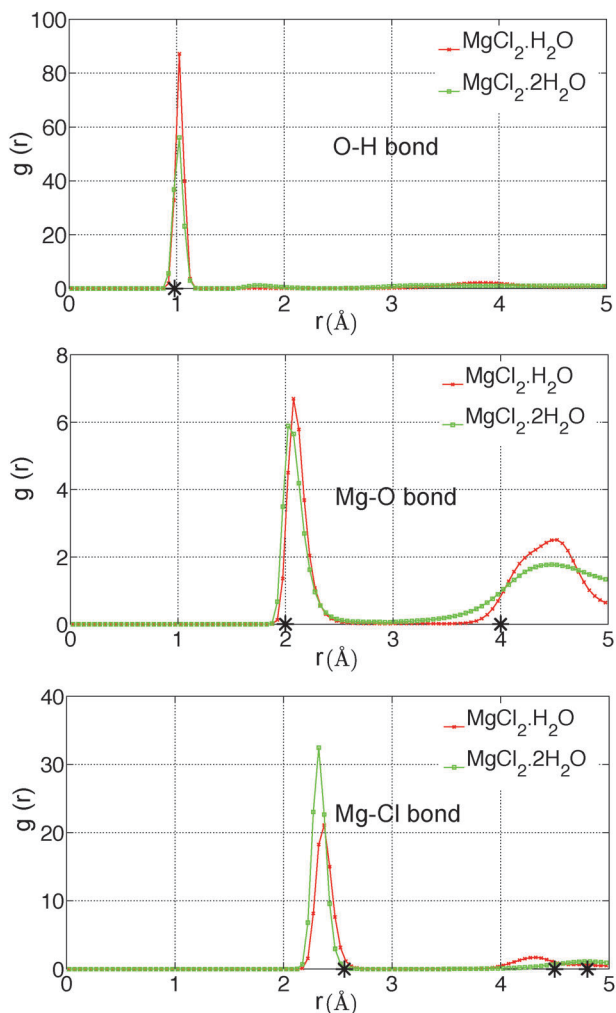
This journal is © the Owner Societies 2016

Phys. Chem. Chem. Phys., 2016, **18**, 15838–15847 | **15843**

Fig. 10 Radial distribution functions of O–H, Mg–O, and Mg–Cl bond in MgCl$_2$·H$_2$O and MgCl$_2$·2H$_2$O obtained with newly developed ReaxFF parameters of MgCl$_2$ hydrates at 300 K. The represents the corresponding distance in the experimental unit cell.[43,44]

Fig. 11 Dehydration kinetics of MgCl$_2$·H$_2$O in a 2D-periodic slab of 26.8 × 21.8 × 1000 Å upto 1 nanosecond using ReaxFF-MD simulations. The solid lines represent the kinetics from ReaxFF-MD simulations while the dashed lines of the same color represent a linear fit to estimate the dehydration rate. N_T is average number of H$_2$O molecules escaping from the slab at temperature T.

the gradient of a linear fit. The dehydration rate keeps on increasing with temperature in the range of 300 to 500 K as shown in Fig. 11. The dehydration rate at 500 K is 3.1 times faster when compared to the rate at 300 K.

The average number of H$_2$O molecules leaving the solid slab of MgCl$_2$·2H$_2$O (44.3 × 1000 × 21.9 Å) into the vacuum region (Y direction) is 51.17 ± 7.63 after 750 picosecond. The system is further equilibrated upto 1000 picosecond and H$_2$O average increased by 4.61. The average density distribution of H$_2$O molecules are obtained by diving the simulation box into the bins of 10 Å along the Y axis as shown in Fig. 9b. Blue lines represent the initial boundaries. The water molecules which escape from the solid slab accumulate on the surface at 300 K. There is a concentration gradient of H$_2$O molecules present on the surface along the Y axis. Thereby, confirms the influence of water diffusion on the dehydration process. The average number of H$_2$O molecules escaping from MgCl$_2$·2H$_2$O increases from 54.93 ± 6.76 to 71.66 ± 7.27 in the temperature range of 300 to 450 K as shown in Fig. 12. Further, increment in

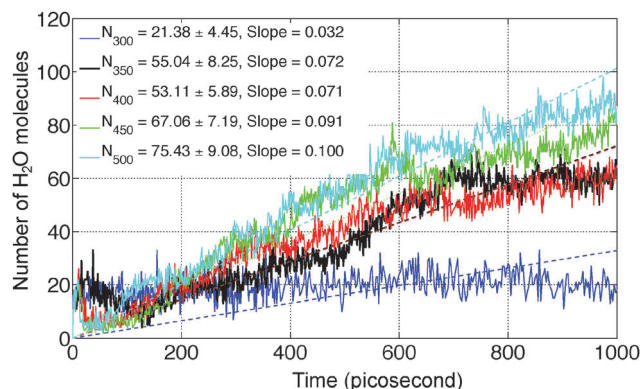temperature leads to reduction in the number of H$_2$O molecules escaping from MgCl$_2$·2H$_2$O to 50.73 ± 5.85 at 500 K as shown in Fig. 12. This reduction in number of water molecules escaping from solid slab of MgCl$_2$·2H$_2$O could be explained from the fact that existing water molecules present in the vacuum region are pushing them back into the crystal. The effect of temperature on the dehydration of MgCl$_2$·H$_2$O and MgCl$_2$·2H$_2$O is similar to experiments.[47]

3.3.3 HCl formation. The HCl formation is investigated at various temperatures (300, 350, 400, 450, and 500 K). The first HCl molecule is observed from the 2D periodic slab of MgCl$_2$·H$_2$O at 350 K after 136.25 picosecond. To narrow down the onset temperature of HCl formation, MD simulations are carried out at the interval of 10 K between 300–350 K. The onset of HCl formation is observed at 340 K after 318.75 picosecond in MgCl$_2$·H$_2$O as shown in Fig. 13b. After dehydration/hydrolysis, the crystal slab elongates along the vacuum direction as some of MgCl$_2$ and H$_2$O came out on the surface. The onset of HCl formation is experimentally[23] observed in the temperature range of 343–353 K, which is in good agreement with the present ReaxFF study. The hydrolysis
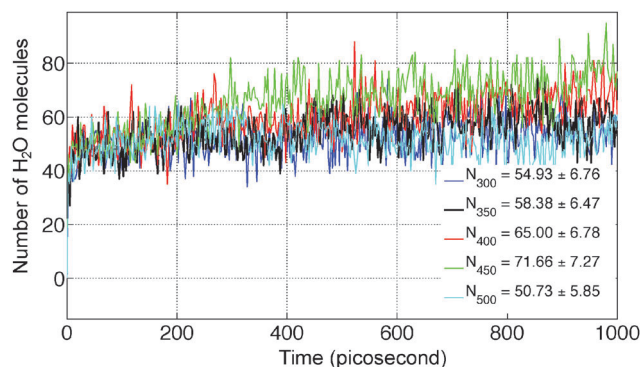

Fig. 12 Dehydration kinetics of MgCl$_2$·2H$_2$O in a 2D-periodic slab of 44.3 × 1000 × 21.9 Å upto 1 nanosecond using ReaxFF-MD simulations. N_T is average number of H$_2$O molecules escaping from the slab at temperature T.
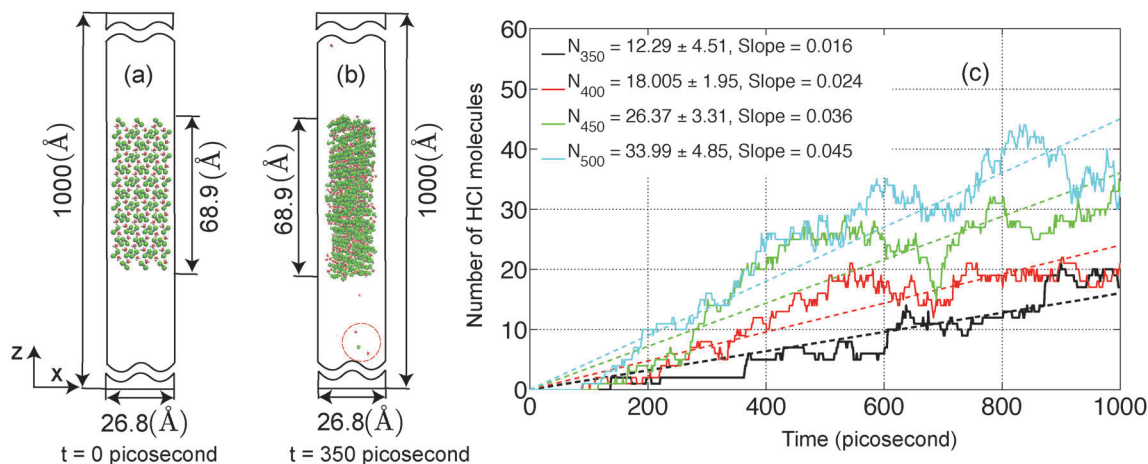
Fig. 13 Side view of $MgCl_2 \cdot H_2O$ in a 2D-periodic slab of $26.8 \times 21.8 \times 1000$ Å used in ReaxFF-MD simulations performed at 340 K (a) initial configuration at $t = 0$ s (b) intermediate configuration at $t = 350$ picosecond. The red dotted circle represents the area where first HCl formations occur. $MgCl_2 \cdot H_2O$ is represented using the ball-and-stick model. Color scheme: Mg = grey, O = red, H = white, and Cl = green (c) hydrolysis kinetics of $MgCl_2 \cdot H_2O$ upto 1 nanosecond. The solid line represents the kinetics from ReaxFF-MD simulation while the dashed line of the same color represents the linear fits to estimate the hydrolysis rate. N_T is average number of HCl molecules escaping from the slab at temperature T.

kinetics of the $MgCl_2 \cdot H_2O$ is shown in Fig. 13c at different temperatures (350–500 K) upto 1000 picosecond. The number of HCl molecules keeps on increasing with temperature. The hydrolysis rate estimated from the linear fits keeps on increasing with temperature as shown in Fig. 13c. The hydrolysis rate at 500 K is 2.8 times faster when compared to the rate at 350 K. Hydrolysis is not observed in $MgCl_2 \cdot 2H_2O$ in the temperature range of 300–500 K.

3.3.4 Effect of the temperature on the H_2O transport. The diffusion of H_2O through a crystalline structure of the solid salt hydrate is a complex phenomena as the H_2O molecules resulting from dehydration reaction have to diffuse to the surface in order to dehydrate. The diffusivity of H_2O is computed from ReaxFF-MD simulations after 250 picosecond of equilibration time and 125 picosecond of production time at various temperatures (300, 350, 400, 450, and 500 K). The DC of H_2O in $MgCl_2 \cdot H_2O$ is 7.18×10^{-11} m^2 s^{-1} at 300 K. The reported DCs in the present study are well converged with VAF interval.

To estimate the statistical error in the DC of H_2O through 2D periodic slabs of $MgCl_2 \cdot H_2O$ and $MgCl_2 \cdot 2H_2O$, five repetitions of ReaxFF-MD simulations are performed with the same parameters at 300 K. The average diffusivity of H_2O through $MgCl_2 \cdot H_2O$ is $7.46 \pm 0.77 \times 10^{-11}$ m^2 s^{-1} and $1.14 \pm 0.15 \times 10^{-10}$ m^2 s^{-1} for $MgCl_2 \cdot 2H_2O$. The DCs in $MgCl_2 \cdot H_2O$ and $MgCl_2 \cdot 2H_2O$ are 0.03 and 0.04 times the DC of bulk water.[48] In the lack of

experimental study for the diffusion of H_2O through $MgCl_2$ hydrates, we compared with the H_2O diffusivity through other TCM epsomite ($MgSO_4 \cdot 7H_2O$).[49] Zhang et al.[49] has reported the same order of magnitude for the diffusivity of H_2O in the center of the $MgSO_4 \cdot 7H_2O$. Donkers et al.[50] has measured the DC of water in epsomite using NMR. They reported the DC in range of 10^{-10} to 10^{-9} m^2 s^{-1} in the temperature range of 293 to 413 K. In the light of their experimental and simulation results of water diffusion in other heat storage material ($MgSO_4 \cdot 7H_2O$), we can conclude that the present ReaxFF-MD simulations could mimic the water transport in $MgCl_2$ hydrates.

To investigate the effect of the temperature, the DC of H_2O through 2D-periodic slabs of $MgCl_2 \cdot H_2O$ and $MgCl_2 \cdot 2H_2O$ are obtained at various temperatures (300, 350, 400, 450, and 500 K). The rise in the temperature increased the thermal energy of H_2O molecules and enhanced the water transport as shown in Table 2. The DC of H_2O through 2D-periodic slabs at various temperatures follow the Arrhenius equation ($D(T) = D_0 \times e^{-[E/RT]}$) with parameters given in Table 3. The activation energy and pre-exponential factor for H_2O diffusion in $MgCl_2 \cdot H_2O$ is higher than $MgCl_2 \cdot 2H_2O$, thus the net effect of the temperature on DC of H_2O through $MgCl_2 \cdot H_2O$ is similar to $MgCl_2 \cdot 2H_2O$. We have fitted the data on water-transport through the epsomite in the temperature range of 293 to 413 K.[50] The DC follows the Arrhenius equation. The activation energy and pre-exponential factor are 5.7×10^{-4} m^2 s^{-1} and 42.6 kcal mol^{-1}. Thus, the strength of Mg–O

Table 2 The diffusion coefficient of water through 2D-periodic slabs at different temperature after 375 picosecond

Temperature, T, K	Diffusivity in $MgCl_2 \cdot H_2O$, m^2 s^{-1}	Diffusivity in $MgCl_2 \cdot 2H_2O$, m^2 s^{-1}
300	6.99×10^{-11}	1.16×10^{-10}
350	7.02×10^{-11}	3.18×10^{-10}
400	9.13×10^{-11}	9.54×10^{-10}
450	6.95×10^{-10}	2.78×10^{-9}
500	4.47×10^{-9}	6.66×10^{-9}

Table 3 Arrhenius parameters for H_2O diffusion through 2D-periodic slabs of $MgCl_2 \cdot H_2O$ and $MgCl_2 \cdot 2H_2O$

Material	Pre exponential factor, D_0 m^2 s^{-1}	Activation energy, kJ mol^{-1}
$MgCl_2 \cdot H_2O$	7.72×10^{-2}	69.28
$MgCl_2 \cdot 2H_2O$	1.55×10^{-5}	32.22

bond in epsomite lies between the strength of Mg–O bond present in $MgCl_2 \cdot H_2O$ and $MgCl_2 \cdot 2H_2O$.

4 Conclusions

To gain more insight into the reaction kinetics of $MgCl_2$ hydrates on molecular level, the development of a new reactive force field (ReaxFF) is desirable. This force field is trained against an extensive set of quantum mechanics data. ReaxFF is optimized against a training set consisting of bond dissociation curve, angle bending curve, enthalpy change in hydrolysis and dehydration reactions and equation of state (EOS). A single-parameter search algorithm in combination with a Metropolis Monte Carlo algorithm is used. The optimized force field is able to reproduce the energy terms along with the computationally challenging EOS of solid crystals. Bulk moduli of $MgCl_2 \cdot H_2O$ and $MgCl_2 \cdot 2H_2O$ obtained from DFT and ReaxFF simulations are in close agreement ($\sim 4\%$ deviation). ReaxFF parameters from the present study represent various chemical bonds like Mg–O, Mg–Cl, and O–H which are in agreement with the DFT and experimental structures.

Barriers of 19.55 kcal mol^{-1} and 29.61 kcal mol^{-1} for proton transfer in $MgCl_2 \cdot 2H_2O$ and $MgCl_2 \cdot 2H_2O$ surrounded by a neighbor H_2O molecule are obtained from DFT calculations. The ReaxFF parameters are able to reproduce the barrier obtained from DFT calculations for the proton transfer in $MgCl_2 \cdot 2H_2O$ (20.27 kcal mol^{-1}) and $MgCl_2 \cdot 2H_2O$ surrounded by a neighbor H_2O molecule (26.54 kcal mol^{-1}). ReaxFF is also able to reproduce the reaction path for the proton transfer. This explains the lower hydrolysis in the higher hydrates (tetra and hexa) of $MgCl_2$ as the neighboring H_2O molecule in higher hydrates increases the barrier for proton transfer and inhibits the hydrolysis. The radial distribution functions for Mg–O, O–H, and Mg–Cl pairs confirm that the optimized force field is able to capture the bonded and non-bonded interactions in the $MgCl_2$ hydrates.

ReaxFF-MD simulations have been carried out on 2D periodic slabs of $MgCl_2 \cdot H_2O$ and $MgCl_2 \cdot 2H_2O$ to investigate the dehydration and hydrolysis kinetics at various temperatures (300–500 K). The average number of H_2O molecules escaping from the $MgCl_2 \cdot H_2O$ slab (after 1 nanosecond) increased from 21.38 ± 4.45 to 75.43 ± 9.08 in the temperature range of 300 to 500 K. The dehydration rate increased 3.1 times in the same temperature range for $MgCl_2 \cdot H_2O$. The onset temperature of HCl formation in $MgCl_2 \cdot H_2O$ is observed to be 340 K, which is in agreement with experiments. Increasing the temperature from 350 to 500 K, we observed that the average number of HCl molecules escaping from the $MgCl_2 \cdot H_2O$ slab (after 1 nanosecond) increased from 12.29 ± 4.51 to 33.99 ± 4.85. The hydrolysis rate increased 2.8 times in the same temperature range for $MgCl_2 \cdot H_2O$. Increasing the temperatures from 300 to 450 K, the average number of H_2O molecules escaping from the $MgCl_2 \cdot 2H_2O$ slab (after 1 nanosecond) increased from 54.93 ± 6.76 to 71.66 ± 7.27. Hydrolysis is not observed from the $MgCl_2 \cdot 2H_2O$ slab in the temperature range of 300–500 K.

The H_2O transport through $MgCl_2 \cdot H_2O$ and $MgCl_2 \cdot 2H_2O$ is investigated using ReaxFF-MD simulations. The diffusion coefficient (DC) of H_2O through $MgCl_2$ hydrates are reported from Green–Kubo method at various temperature ranging from 300–500 K. The DC of H_2O in the present study is of the same order of magnitude as the DC of H_2O in $MgSO_4 \cdot 7H_2O$ obtained both from MD simulations[49] and experiments.[50] The DC increases with temperature and follows the Arrhenius law for $MgCl_2 \cdot H_2O$ and $MgCl_2 \cdot 2H_2O$. The diffusivity of H_2O through $MgCl_2 \cdot H_2O$ at 500 K increases 64 times compared with diffusivity at 300 K. Similarly, the diffusivity of H_2O through $MgCl_2 \cdot 2H_2O$ at 500 K increased 57 times compared to the 300 K. The diffusivity trend suggests that by increasing the temperature upto 500 K, the H_2O transport (mass diffusion) can be improved. These results demonstrate the ability of ReaxFF to explore the molecular reaction rate for dehydration/hydrolysis of $MgCl_2$ hydrates along with the water transport in the operational range of seasonal heat storage systems.

Acknowledgements

References

1 K. E. N'Tsoukpoe, H. Liu, N. Le Pierrès and L. Luo, *Renewable Sustainable Energy Rev.*, 2009, **13**, 2385–2396.

2 A. H. Abedin and M. A. Rosen, *Open Renewable Energy J.*, 2011, **4**, 42–46.

3 J. Xu, R. Wang and Y. Li, *Sol. Energy*, 2014, **103**, 610–638.

4 D. Aydin, S. P. Casey and S. Riffat, *Renewable Sustainable Energy Rev.*, 2015, **41**, 356–367.

5 A. J. Carrillo, D. Sastre, D. P. Serrano, P. Pizarro and J. M. Coronado, *Phys. Chem. Chem. Phys.*, 2016, **18**, 8039–8048.

6 K. E. N'Tsoukpoe, T. Schmidt, H. U. Rammelberg, B. A. Watts and W. K. Ruck, *Appl. Energy*, 2014, **124**, 1–16.

7 H. Zondag, V. Van Essen, L. Bleijendaal, B. Kikkert and M. Bakker, Proceedings IRES 2010 conference, Berlin, 2010.

8 B. Smeets, E. Iype, S. Nedea, H. Zondag and C. Rindt, *J. Chem. Phys.*, 2013, **139**, 124312.

9 A. El-Sebaii, S. Al-Amir, F. Al-Marzouki, A. S. Faidah, A. Al-Ghamdi and S. Al-Heniti, *Energy Convers. Manage.*, 2009, **50**, 3104–3111.

10 H. U. Rammelberg, T. Schmidt and W. Ruck, *Energy Procedia*, 2012, **30**, 362–369.

11 A. El-Sebaii, S. Al-Heniti, F. Al-Agel, A. Al-Ghamdi and F. Al-Marzouki, *Energy Convers. Manage.*, 2011, **52**, 1771–1777.

12 P. F. Weck and E. Kim, *J. Phys. Chem. C*, 2014, **118**, 4618–4625.

13 R. Pilar, L. Svoboda, P. Honcova and L. Oravova, *Thermochim. Acta*, 2012, **546**, 81–86.

15846 | *Phys. Chem. Chem. Phys.*, 2016, **18**, 15838–15847

This journal is © the Owner Societies 2016

14 G. J. Kipouros and D. R. Sadoway, *J. Light Metals*, 2001, **1**, 111–117.

15 L. Guangming, M. Peihua, W. Zhiming, L. Mingzhen and C. Minxong, *Thermochim. Acta*, 2004, **412**, 149–153.

16 W. Wang and S. Chen, *Journal of Computational Science & Engineering*, 2011, **2**, 79–84.

17 Q. Huang, G. Lu, J. Wang and J. Yu, *J. Anal. Appl. Pyrolysis*, 2011, **91**, 159–164.

18 E. Iype, S. V. Nedea, C. C. M. Rindt, A. A. van Steenhoven, H. A. Zondag and A. P. J. Jansen, *J. Phys. Chem. C*, 2012, **116**, 18584–18590.

19 S. Shoval, S. Yariv, Y. Kirsh and H. Peled, *Thermochim. Acta*, 1986, **109**, 207–226.

20 Y. Kirsh, S. Yariv and S. Shoval, *J. Therm. Anal.*, 1987, **32**, 393–408.

21 A. K. Galwey and G. M. Laverty, *Thermochim. Acta*, 1989, **138**, 115–127.

22 M. Dittner, J. Müller, H. M. Aktulga and B. Hartke, *J. Comput. Chem.*, 2015, **36**, 1550–1561.

23 C. Ferchaud, R. Scherpenborg, L. Scapino, J. Veldhuis, H. Zondag and R. D. Boer, Proceedings of the Advances in Thermal Energy Storage, Lleida, Spain, 2014.

24 S. Lan, H. Zondag, A. van Steenhoven and C. Rindt, *J. Therm. Anal. Calorim.*, 2016, 1–10.

25 A. Pathak, S. Nedea, C. Rindt, D. Smeulders and H. Zondag, Proceedings NEGF 2015 conference, Eindhoven, 2015.

26 A. C. Van Duin, S. Dasgupta, F. Lorant and W. A. Goddard, *J. Phys. Chem. A*, 2001, **105**, 9396–9409.

27 K. Chenoweth, A. C. v. Duin, P. Persson, M.-J. Cheng, J. Oxgaard and W. A. Goddard, III, *J. Phys. Chem. C*, 2008, **112**, 14645–14654.

28 J. Ojwang, R. Van Santen, G. J. Kramer, A. C. van Duin and W. A. Goddard III, *J. Chem. Phys.*, 2008, **128**, 164714.

29 D. Raymand, A. C. van Duin, M. Baudin and K. Hermansson, *Surf. Sci.*, 2008, **602**, 1020–1031.

30 J. Ojwang, R. A. van Santen, G. J. Kramer, A. C. van Duin and W. A. Goddard III, *J. Chem. Phys.*, 2009, **131**, 044501.

31 K. Chenoweth, A. C. van Duin and W. A. Goddard, *J. Phys. Chem. A*, 2008, **112**, 1040–1053.

32 A. C. van Duin, J. M. Baas and B. van de Graaf, *J. Chem. Soc., Faraday Trans.*, 1994, **90**, 2881–2895.

33 E. Iype, M. Hütter, A. Jansen, S. V. Nedea and C. Rindt, *J. Comput. Chem.*, 2013, **34**, 1143–1154.

34 G. Te Velde, F. M. Bickelhaupt, E. J. Baerends, C. Fonseca Guerra, S. J. van Gisbergen, J. G. Snijders and T. Ziegler, *J. Comput. Chem.*, 2001, **22**, 931–967.

35 A. D. Pathak, S. Nedea, H. Zondag, C. Rindt and D. Smeulders, *Phys. Chem. Chem. Phys.*, 2016, 10059–10069.

36 G. Kresse and J. Furthmüller, *Phys. Rev. B: Condens. Matter Mater. Phys.*, 1996, **54**, 11169.

37 P. E. Blöchl, *Phys. Rev. B: Condens. Matter Mater. Phys.*, 1994, **50**, 17953.

38 J. P. Perdew, K. Burke and M. Ernzerhof, *Phys. Rev. Lett.*, 1996, **77**, 3865.

39 T. Liang, Y. K. Shin, Y.-T. Cheng, D. E. Yilmaz, K. G. Vishnu, O. Verners, C. Zou, S. R. Phillpot, S. B. Sinnott and A. C. van Duin, *Annu. Rev. Mater. Res.*, 2013, **43**, 109–129.

40 J. E. Mueller, A. C. T. van Duin and I. William A. Goddard, *J. Phys. Chem. C*, 2010, **114**, 4939–4949.

41 G. Mazenko, J. Banavar and R. Gomer, *Surf. Sci.*, 1981, **107**, 459–468.

42 R. Wyckoff, *Cryst. Struct.*, 1963, **1**, 239–444.

43 K. Sugimoto, R. E. Dinnebier and J. C. Hanson, *Acta Crystallogr., Sect. B: Struct. Sci.*, 2007, **63**, 235–242.

44 J. A. Kaduk, *Acta Crystallogr., Sect. B: Struct. Sci.*, 2002, **58**, 370–379.

45 http://www.crystallography.net/.

46 A. L. Kaledin, A. C. van Duin, C. L. Hill and D. G. Musaev, *J. Phys. Chem. A*, 2013, **117**, 6967–6974.

47 C. Ferchaud, PhD thesis, Eindhoven University of Technology, 2016.

48 E. Chiavazzo, M. Fasano, P. Asinari and P. Decuzzi, *Nat. Commun.*, 2014, **5**.

49 H. Zhang, E. Iype, S. V. Nedea and C. C. Rindt, *Mol. Simul.*, 2014, **40**, 1157–1166.

50 P. A. J. Donkers, S. Beckert, L. Pel, F. Stallmach, M. Steiger and O. C. G. Adan, *J. Phys. Chem. C*, 2015, **119**, 28711–28720.

This journal is © the Owner Societies 2016

Phys. Chem. Chem. Phys., 2016, **18**, 15838–15847 | **15847**